Int. J. Electrochem. Sci., 14 **(2019)** 1107 – 1115, doi: 10.20964/2019.02.21

International Journal of ELECTROCHEMICAL SCIENCE
www.electrochemsci.org

Composite Comprising β-Sn and Amorphous Mn Phases Formed by Phase Separation during Electrodeposition

M. Saitou

University of the Ryukyus, Department of Mechanical Systems Engineering, 1 Senbaru Nishihara-cho Okinawa, 903-0213, Japan.
*E-mail: saitou@tec.u-ryukyu.ac.jp

Received: 1 November 2018 / *Accepted:* 29 November 2018 / *Published:* 5 January 2019

Sn–Mn thin films electrodeposited in aqueous solutions having Mn/Sn charged molar ratios between 0.05 and 3.5 within a temperature range from 273 to 323 K were investigated using energy dispersive X-ray spectroscopy (EDX) and X-ray diffraction (XRD). A Mn/Sn critical charged molar ratio at which the Mn contents in the Sn–Mn thin films appreciably changed was observed. The Mn/Sn critical charged molar ratio shifted to a larger value with an increase in the deposition temperature. The EDX and XRD analyses demonstrated that the electrodeposited Sn–Mn thin films comprised β-Sn and amorphous Mn phases, and the β-Sn phase and the amorphous Mn phase formed by the phase separation at the Mn/Sn critical charged molar ratio. In addition, the Sn–Mn thin films did not include any intermetallic compounds. The Sn–Mn thin films were concluded to be composites comprising the β-Sn and amorphous Mn phases. The phase separation and the Mn/Sn critical charged molar ratio were explained by a free energy model.

Keywords: Critical charged molar ratio; β-Sn: Amorphous Mn; Phase separation; Composite; Free energy model

1. INTRODUCTION

Heusler compounds [1–4] are promising candidates having wide applications in spintronics owing to their magneto-caloric effect, magnetoresistance, magnetic anisotropy, and magnetic shape effect. Many experimental studies demonstrated that their crystal structure, composition, and heat treatment affected the magnetic properties of Heusler compounds. The Heusler compounds including Sn and Mn have the general formula X_2YZ, for example, Ni_2MnSn and Co_2MnSn. To form the Heusler compounds, electrodeposition [5–6] is a useful method because of easy deposition from aqueous

solutions and the control of the stoichiometry ratios using electrochemical parameters such as the current density, frequency, and solution conditions.

Sn–Mn- based materials have recently gained attention from researchers as a new anode material for Li-ion batteries [7–10]. Sn anodes have superior performance in terms of specific and volumetric capacities as compared to porous graphite currently used for anodes in Li-ion batteries. Mn is considered to overcome the pulverization due to the huge volume change caused by repeated cycles of lithiation and delithiation. Further, the inactive Mn element is expected to play the important role of a buffer that reduces the stress induced by the change in volume during the repeated cycles.

Sn–Mn thin films have often been prepared using electrodeposition. X-ray diffraction patterns of Sn–Mn electrodeposits [11–13] demonstrated diffraction peaks from not only β-Sn and γ-Mn, but also intermetallic compounds of Sn and Mn such as MnO, MO_2, $Mn(OH)_2$, SnO, and $MnSn_2$. Sn–Mn thin films including the intermetallic compounds have disadvantages in applications to the Heusler compounds and the Sn–Mn- based anode materials. These intermetallic compounds significantly reduce the experimental values of specific and volumetric capacities compared with their theoretical values. Hence, a new electrochemical method to produce Sn-Mn thin films comprising Sn phases and Mn phases is desirable.

The aims of the present study are to obtain a Mn/Sn critical charged molar ratio at which the β-Sn phase and amorphous Mn phase are formed by the phase separation and develop a method to form Sn–Mn thin film composites comprising only the β-Sn phases and the amorphous Mn phases.

2. EXPERIMENTAL SETUP

A copper plate of 30×10 mm^2 and a carbon plate of 50×40 mm^2 were used as the cathode and anode, respectively. One side of the copper plate was electrically insulated to generate a Sn–Mn electrodeposit only on the other side. Aqueous solutions including the following chemical compounds (mol L^{-1}) were prepared: $SnSO_4$ (0.178–0.762), $MnSO_4 \cdot 4H_2O$ (0.038–0.622) and $KNaC_4H_4O_6 \cdot 4H_2O$ (0.55). The Mn/Sn charged molar ratios in the aqueous solutions were within a range from 0.05 to 3.5. The aqueous solution was strained using a membrane filter to remove Sn and Mn hydroxide particles. The cathode and anode were placed parallel to each other in a cell filled with the aqueous solution, which was maintained within a temperature range from 273 to 323 K during electrodeposition using a Peltier controller. A rectangular pulse current within a frequency range from 0.4 to 1.2 MHz was supplied to the cell by a function generator. A metal film resistor of 22 Ω was connected in series with the cell to calculate the current flowing to the cell. The rectangular pulse current with an amplitude of 22 mA cm^{-2} was employed. Figure 1 shows a 0.8 MHz rectangular pulse current with an amplitude of 22 mA cm^{-2}.

After the electrodeposition, the Sn–Mn thin film electrodeposited on the copper plate was rinsed with distilled water and dried. The Sn–Mn thin film was weighted to a precision of 0.1 mg with an electric balance to calculate the thickness of the Sn–Mn thin film. A mapping of Sn and Mn elements in the Sn–Mn thin film was conducted using energy dispersive X-ray spectroscopy (EDX) (Hitachi TM3030). Diffractions from the crystallographic planes in the Sn–Mn thin film were investigated using a conventional X-ray diffraction (XRD) (Rigaku Ultima) with CuKα radiation.

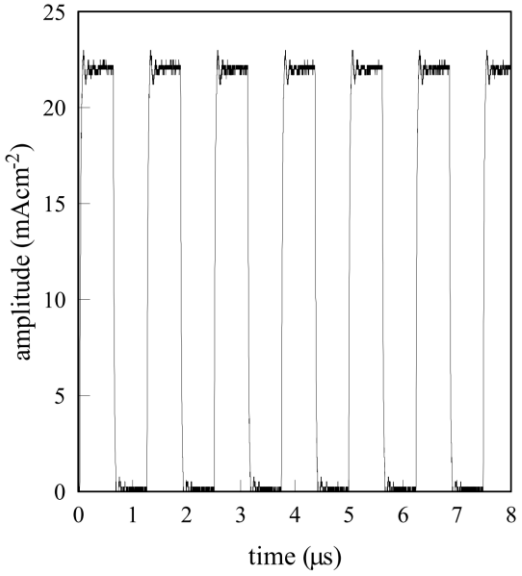

Figure 1. Rectangular pulse current with an amplitude of 22 mA cm^{-2} and frequency of 0.8 MHz.

3. RESULTS AND DISCUSSION

3.1. Rapid change in Mn contents in Sn-Mn thin films

Figure 2 shows the Mn content in the Sn–Mn thin films electrodeposited at 303 K within a frequency range from 0.4 to 0.7 MHz. The Sn–Mn thin films were generated from the aqueous solution with the Mn/Sn charged molar ratio of 2.0. An oscillatory change in the Mn content occurred between 92.1 and 98.3 wt%. The oscillatory change in the metal element in electrodeposits generated at megahertz frequencies has been reported to occur at a resonant frequency because of an energy level transition [14]. Thus, when the energy level transition between the Fermi energy level of electron in the Cu plate and the quantized rotational energy level of a complex ion comprising Mn and tartrate ions occurs, the Mn content has a maximum value at the resonant frequency.

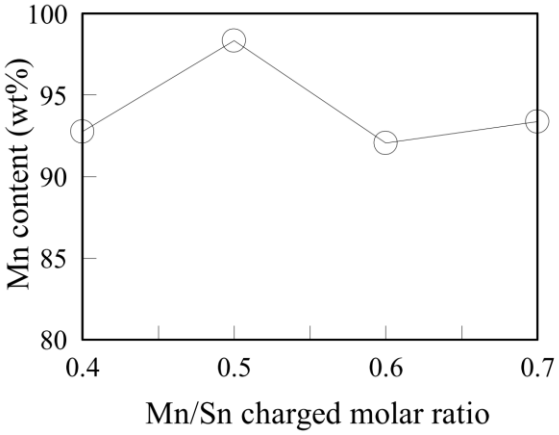

Figure 2. A plot of the Mn content in the Sn–Mn thin films electrodeposited at 303 K within a frequency range from 0.4 to 0.7 MHz using the aqueous solution including the Mn/Sn charged molar ratio of 2.

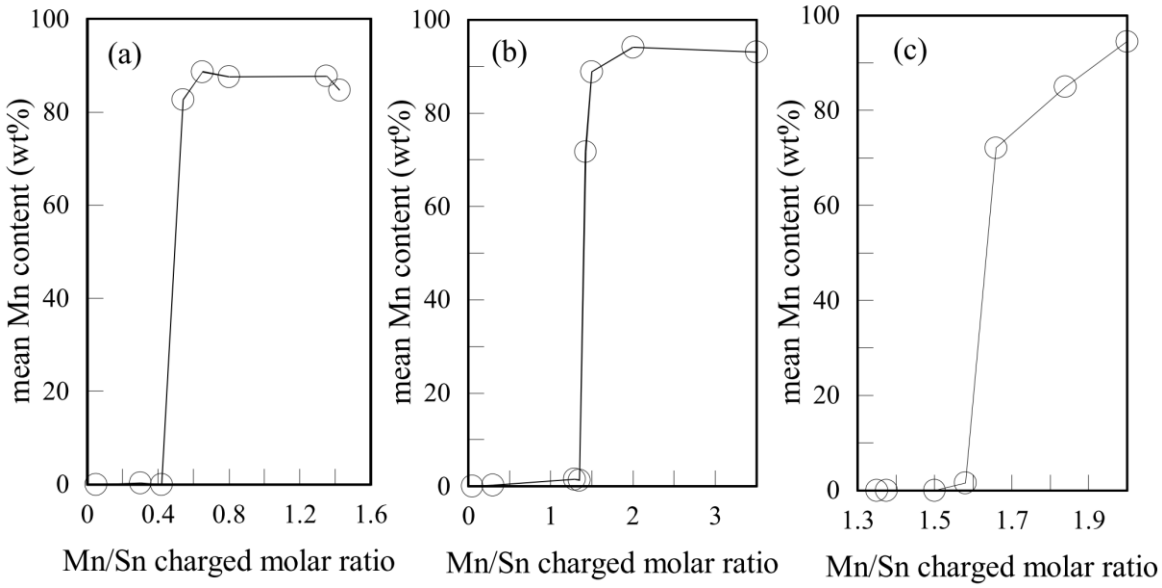

Figure 3. Plots of the Mn content in the Sn–Mn thin films vs. the Mn/Sn charged molar ratio in aqueous solutions at a deposition temperature of (a) 273 K, (b) 303 K, and (c) 323 K.

Figure 3 shows plots of the mean Mn content in Sn–Mn thin films vs. the Mn/Sn charged molar ratio in the solutions. The mean Mn content denotes the value of the Mn content in the Sn–Mn thin films averaged over the frequencies. In Fig. 3 (a), the mean Mn content in the Sn–Mn thin films electrodeposited at 273 K was 0.1 wt% when the Mn/Sn charged molar ratio was less than 0.42. The mean Mn content rapidly changed at the Mn/Sn charged molar ratio of 0.54 and increased by 82.0 wt%. As the Mn/Sn charged molar ratio increased further, the mean Mn content reached approximately 87 wt%. In Fig. 3 (b), the mean Mn content in Sn–Mn thin films electrodeposited at 303 K became 0.8 wt% when the Mn/Sn charged molar ratio was less than 1.35. Similar to the Mn content in Fig. 3 (a), the Mn content rapidly changed at the Mn/Sn charged molar ratio of 1.5 and became 88.9 wt%. At a Mn/Sn charged molar ratio larger than 1.5, the Mn content became 93 wt%. In Fig. 3 (c), the mean Mn content in the Sn–Mn thin films electrodeposited at 323 K reached 0.4 wt% when the Mn/Sn charged molar ratio was less than 1.58. The mean Mn content rapidly increased at the Mn/Sn charged molar ratio of 1.66 and became 72.1 wt%.

These rapid changes in the mean Mn content occur in a manner similar to a phase transition. The transition was characterized by a change in the phases, which occurred in an extremely narrow region of the charged molar ratio, to determine that it was dependent on the deposition temperature. As shown in Fig. 3, we here define the Mn/Sn critical charged molar ratio at which the Mn content in Sn–Mn thin films rapidly changes. In Fig. 3, the Mn/Sn critical charged molar ratios for 273, 303, and 323 K were 0.48, 1.39, and 1.54 respectively. The critical charged molar ratio seemed to shift to a larger molar ratio value with an increase in the deposition temperature.

Figure 4 shows a plot of the Mn/Sn critical charged molar ratio vs. the deposition temperature. The critical charged molar ratio increased with the deposition temperature. In general, the critical behavior is interpreted on the basis of free energy. To discuss the transition in the following section, the

phases and their crystallographic structures of electrodeposited Sn–Mn thin films were required to be determined.

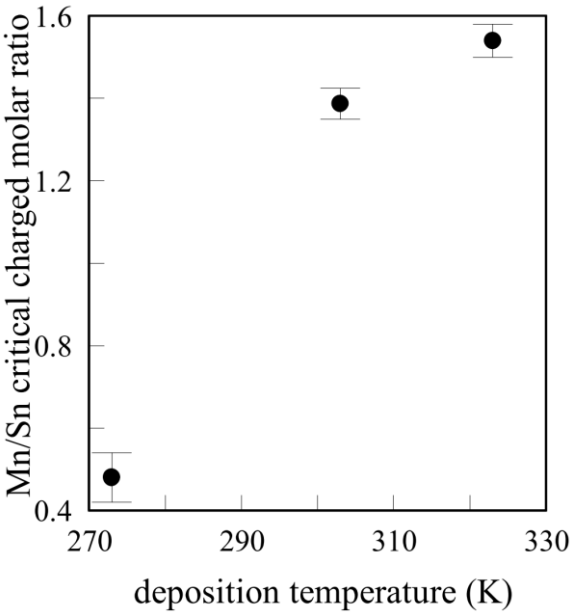

Figure 4. Dependence of the Mn/Sn critical charged molar ratio on the deposition temperature.

3.2. Formation of β-Sn and amorphous phases by the phase separation

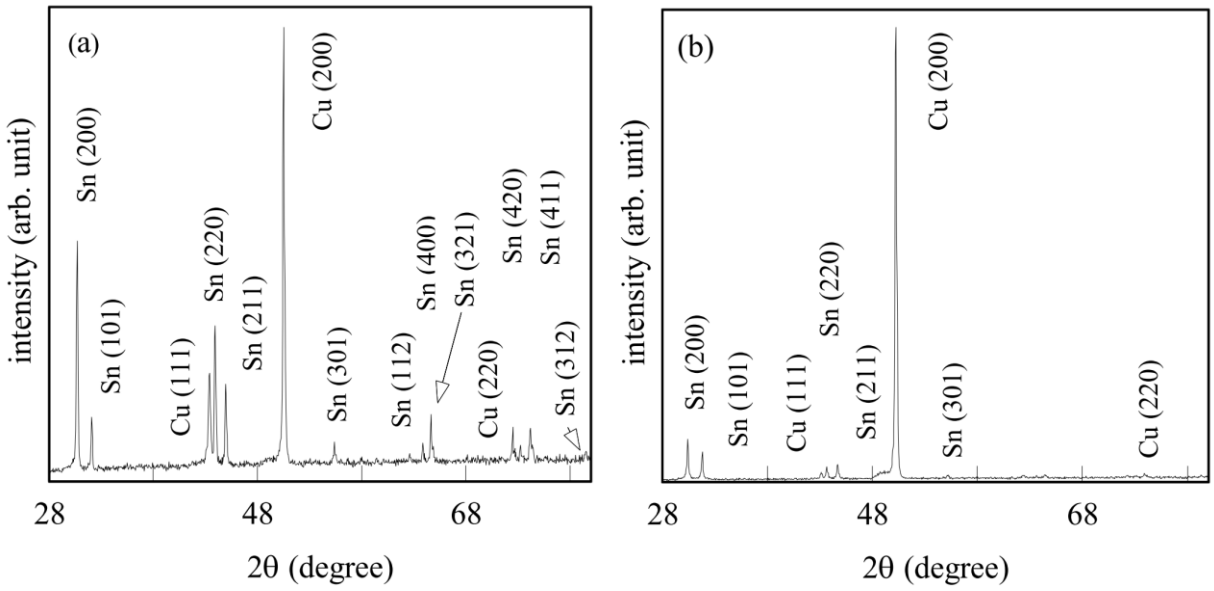

Figure 5. XRD patterns of the Sn–Mn thin films electrodeposited at 303 K and 0.4 MHz using the aqueous solutions with the Mn/Sn charged molar ratios of (a) 1.35 and (b) 1.5. The Sn–Mn films were (a) 3.1 μm thick and (b) 11.5 μm thick.

Figure 5 shows the typical XRD patterns of the Sn–Mn thin films electrodeposited at 303 K. The Mn/Sn charged molar ratios in the solutions were (a) 1.35 and (b) 1.5. In Fig. 5 (a), eleven diffraction peaks indexed as Sn crystallographic planes indicated that the Sn–Mn thin films included β-Sn. The

mean Mn content in the Sn–Mn thin film was 1.3 wt%. According to the Sn–Mn phase diagram at the Mn content of 1.3 wt% [15], a β-Sn phase and a $MnSn_2$ intermetallic phase coexist at room temperature. Diffraction peaks from not only $MnSn_2$ [16], but also other intermetallic compounds such as MnO, MO_2, $Mn(OH)_2$, and SnO have often been reported in many studies [11–13, 17]. However, the intermetallic compounds did not appear in Fig. 5 (a). Consequently, Fig. 5 simply demonstrated that the diffraction peaks from only the β-Sn phase were observed.

In this study, the time period during which the current flowed to the cell within one cycle comprising turn-on and off times as shown in Fig. 1 was within a range from 0.417 to 1.25 μs. Hence, the reaction time required to generate the intermetallic compounds in electrodeposition might be longer than the time period. In addition, despite the mean Mn content of 1.3 wt%, no diffraction peak from the β-Mn phase was observed in the XRD pattern.

In Fig. 5 (b), five weak diffraction peaks indexed as Sn crystallographic planes at the Mn/Sn charged molar ratio of 1.5 indicated that the Sn–Mn thin films slightly included the β-Sn phases. According to the EDX analysis in Fig. 3 (b), the mean Mn content in the Sn–Mn thin film was 88.9 wt%. In the Sn–Mn phase diagram at the Mn content of 88.9 wt%, an α-Mn phase and a β-Mn phase co-exist at room temperature. However, in spite of the Sn–Mn thin film with 11.5 μm thickness, no diffraction peak from the Mn phases appeared in Fig. 5 (b). This indicated that the crystallographic structure of the Mn phase in the Sn–Mn thin film had an amorphous structure [18]. No diffraction peak from the intermetallic compounds [11–13, 17] appeared in Fig. 5. The Sn–Mn thin films were concluded to be composites comprising the β-Mn and amorphous Mn phases. These results were not predicted from the Sn–Mn phase diagram.

As we reported that no α-Sn phase was electrodeposited within a temperature range from 273 to 282 K [19], the stable phases formed in electrodeposition were different from those in the Sn phase diagram. Sn and Mn atoms that crystallized from their ions in a solution might have different free energies from Sn and Mn atoms in solid phases as shown in the Sn–Mn phase diagram [15]. The alloying behavior between Sn and Mn atoms was not observed in our system.

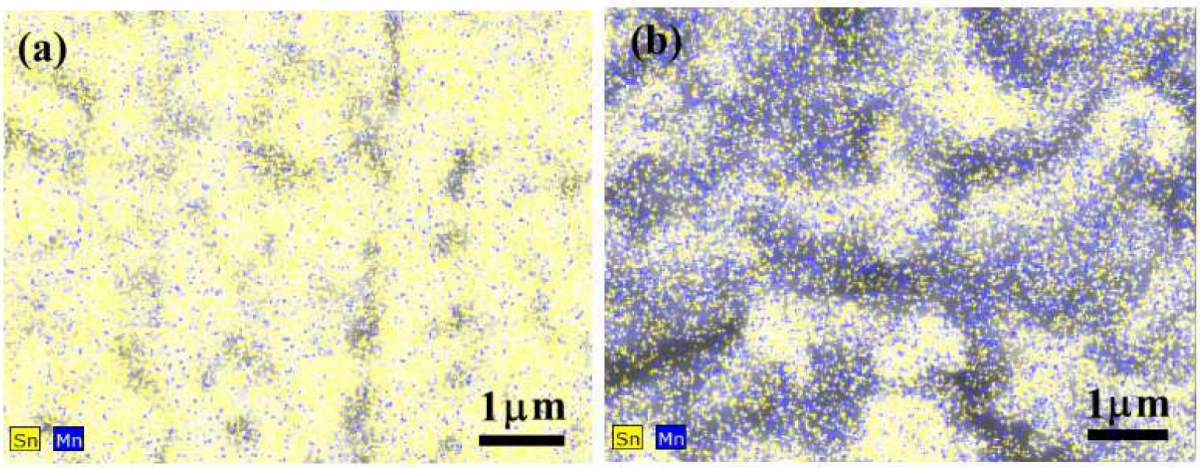

Figure 6. Sn and Mn element mapping analysis of the Sn–Mn thin films electrodeposited at 303 K and 0.4 MHz in the aqueous solutions including the Mn/Sn charged molar ratios of (a) 1.35 and (b) 1.5 using EDX.

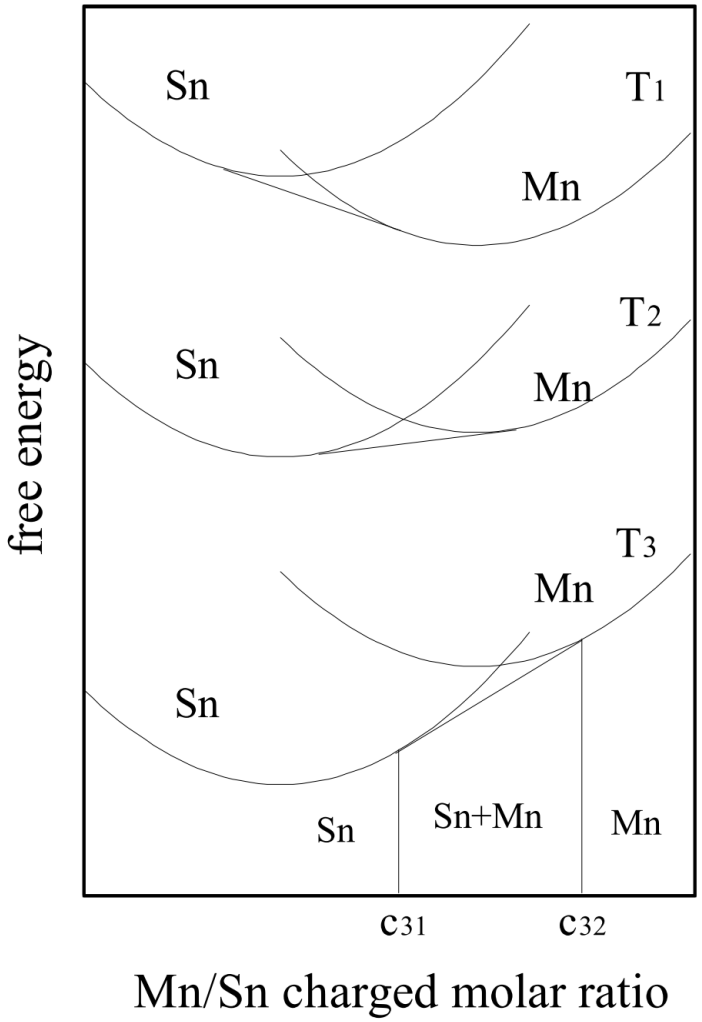

Figure 7. Free energy model to explain the phase separation and the critical charged molar ratio where T_i is the deposition temperature ($T_1<T_2<T_3$).

Figure 6 shows mapping images of Sn and Mn elements in the Sn–Mn thin films electrodeposited in the solutions with the Mn/Sn charged molar ratios of (a) 1.35 and (b) 1.5 at 303 K. The EDX (TM3030) used a 15 kV accelerated electron beam as a probe. The penetration depth of electrons in the Sn-Mn film was presumed to be approximately 1.5 μm [20]. Hence, it was difficult to obtain an element mapping image where the Sn and Mn phases were completely separated. In Fig. 5 (a), the Sn and Mn phases were observed to be roughly separated. Similarly, in Fig. 6 (b) the Sn and Mn phases were also roughly separated. As shown in Fig. 6, the Sn–Mn thin films did not form an alloy of Sn and Mn. The XRD and EDX analysis indicated that the phase separation occurred at the Mn/Sn critical charged molar ratio when Sn and Mn were co-electrodeposited in our system.

Figure 7 shows a free energy model to explain the phase separation in Sn–Mn thin films. Let us consider the free energy of the solution including two compositions such as a complex ion comprising a Mn ion and tartrate ion, and water molecule. Analogous with the free energy of a binary solid solution [21], the free energy of the solution in this study has a curve convexed downward and a minimum value. Similarly, the free energy of a Sn ion and tartrate ion has a curve convexed downward and a minimum

value. The tangent lines to the free energy curves [21] of Sn and Mn are drawn at a temperature of T_1, T_2, and T_3 ($T_1<T_2<T_3$). Here, as the temperature increases, we assume that the free energy of Mn gradually increases compared with that of Sn. As shown in the free energy curve at a temperature of T_3, the phase separation occurs between c_{31} and c_{32} where c_{31} and c_{32} are the charged molar ratios. This is because the free energy is reduced owing to the phase separation. If the difference between c_{31} and c_{32} is significantly small, the phase separation occurs in a manner similar to the phase transition. In addition, as the deposition temperature increases, the critical charged molar ratio shifts to a larger value as shown in Fig. 7. Thus, the dependence of the critical charged molar ratio on the deposition temperature was explained.

4. CONCLUSIONS

The Sn–Mn thin films were electrodeposited using the aqueous solutions having the Mn/Sn charged molar ratios between 0.05 and 3.5 within a deposition temperature range from 273 to 323 K. The phase separation into the Sn and Mn phases was observed to occur at the Mn/Sn critical charged molar ratio. The critical charged molar ratio Mn/Sn increased with the deposition temperature. The formation of intermetallic compounds and the alloying of Sn and Mn atoms were not observed according to the EDX and XRD analyses. The Sn–Mn thin film was concluded to be a composite comprising only the β-Sn phases and the amorphous Mn phases. The phase separation and the critical charged molar ratio were explained by the free energy model.

References

1. M. Yin and P. Nash, *J. Alloys Compd.*, 667 (2016) 184.
2. I. Galanakis, Ph. Mavropoulos, and P. H. Dederichs, *J. Phys. D: Appl. Phys.*, 39 (2006) 765.
3. R. Modak, B. Samantaray, P. Mandal, and A. Srinivasan, *J. Alloys Compd.*, 692 (2017) 529
4. V. V. Marchenkov, Yu. A. Perevozchikova, N. I. Kourov, V. Yu. Irkhin, M. Eisterer, and T. Gao, *J. Magn. Magn. Mater.*, 459 (2018) 211.
5. S. Khan, N. Ahmad, N. Ahmed, and X. F. Han, *J. Magn. Magn. Mater.*, 460 (2018) 120.
6. S. Gao, Y. Liu, and X. Kou, *Int. J. Electrochem. Sci.*, 10 (2015) 8727.
7. Y. He, L. Xu, C. Li, X. Chen, G. Xu, and X. Jiao, *Nano Research*, 11 (2018) 3555.
8. R. Zhang, G. Fang, W. Liu, B. Xia, H. Sun, J. Zheng, and D. Li, *Appl. Surf. Sci.*, 292 (2014) 682.
9. A. Mahmoud, M. Chamas, J-C. Jumas, B. Philippe, R. Dedryvère, D. Gonbeau, I. Saadoune, and P-E. Lippens, *J. Power Sources*, 244 (2013) 246.
10. X. J. Zhu, Z. P. Guo, P. Zhang, G. D. Du, C. K. Poh, Z. X. Chen, S. Li, and H. K. Liu, *Electrochim. Acta*, 55 (2010) 4982.
11. J. Gong and G. Zangai, *Mater. Sci. Eng.*, A344 (203) 268.
12. N. Ivanova, *Electrochem. Commun.*, 80 (2017) 48.
13. H. Kazimierczak, P. Ozga, M. Słupska, Z. Świątek, and K. Berent, *J. Electrochem. Soc*., 161 (2014) D309.
14. M. Saitou, *Int. J. Electrochem. Sci.*, 13 (2018) 305.
15. H. Okamoto, *J. Phase Equilibria*, 20 (1999) 542.
16. T. F. Duan, W. J. Ren, W. Liu, and Z. D. Zhang, *Phys. B*, 495 (2016) 94.

17. N. M. Pereira, C. M. Pereira, J. P. Araújo, and A. F. Silva, *J. Electrochem. Soc.*, 164 (2017) D486.
18. J. Gong, I. Zana, and G. Zangari, *J. Mater. Sci. Lett.*, 20 (2001) 1921.
19. M. Saitou, *Int. J. Electrochem. Sci.*, 13 (2018) 3326.
20. I. Prencipe, D. Dellasega, A. Zani, D. Rizzo, and M. Passoni, *Sci. Technol. Adv. Mater.*, 16 (2015) 025007.
21. J. D. Verhoeven, Fundamentals of Physical Metallurgy (1975), John Willey & Sons, New York, USA.